

A Time-Domain Surface Integral Technique for Mixed Electromagnetic and Circuit Simulation

Chuanyi Yang, *Member, IEEE*, and Vikram Jandhyala, *Senior Member, IEEE*

Abstract—This paper presents a coupled simulation approach in the time domain for modeling nonlinear circuits, electromagnetic components, and electromagnetic interference (EMI) interactions together in one integrated methodology. The approach is based on a rigorous coupling of circuit simulation and time-domain integral equation simulation. The method obviates the need for circuit realizations of electromagnetic interactions, and can be considered complementary to the partial element equivalent circuits, for cases where surface-based modeling is preferable such as complex connectors and packages, and for Green's function based modeling of skin effects.

Index Terms—Coupled circuit-electromagnetic (EM) simulation, electromagnetic interference (EMI), modified nodal analysis, surface impedance, time-domain integral equation (TDIE).

I. INTRODUCTION

TIME-DOMAIN electromagnetic solvers are useful for simulating coupled circuit-electromagnetic (EM) problems involving integrated circuit packages and systems-on-chip, wherein effects of nonlinearities of circuit elements can be modeled accurately [1]–[3]. The surface-based time-domain integral equation (TDIE) approach has been gaining in popularity owing to its flexibility in modeling arbitrarily shaped structures and its enhanced computational performance due to advances in fast solution methods [2]–[6].

Existing methods to couple TDIE formulations to circuits have been based on port models, convolution methods, and the partial element equivalent circuit (PEEC) approach [7]–[10]. However, a seamless approach to integrate circuit and EM interactions without converting to circuits has not been developed within the scope of surface-based TDIEs, that have the advantage of modeling arbitrarily shaped structures with surface-only formulations, and of incorporating skin effects automatically with no volumetric meshing.

In this paper, a generalized rigorous coupling scheme, to simultaneously simulate circuits with SPICE-like time-domain simulation, and EM interactions with a TDIE method, is presented. To efficiently model conductors with finite conductivity, the well-known surface impedance approximation [11], [12] for modeling skin effects is implemented. In the time domain, this

Manuscript received January 31, 2003; revised November 16, 2004. This work was supported in part by the Defense Advanced Research Projects Agency-Microsystems Technology Office under NeoCAD Grant N66001-01-1-8920, by the National Science Foundation under CAREER Grant ECS-0093102, by the National Science Foundation-Semiconductor Research Corporation under Mixed-Signal Initiative Grant CCR-0120371, and by a grant from the Ansoft Corporation.

The authors are with the Applied Computational Electromagnetics Laboratory, Department of Electrical Engineering, University of Washington, Seattle WA 98195 USA (e-mail: jandhyala@ee.washington.edu).

Digital Object Identifier 10.1109/TADVP.2005.848389

has been widely used and tested in finite difference time-domain methods and transmission line simulation [13]–[16]. This approach enables direct solution of circuit-EM equations without the need for generating port models. The method permits both circuit and EM excitations and thereby has potential as a signal integrity and as an EMI/electromagnetic compatibility (EMC) modeling tool. This approach may be useful as a complement to PEEC-like approaches, for cases where arbitrarily shaped packaging and component structures need to be modeled, and skin effects are important. The approach is also a rigorous coupled EM-circuit coupling scheme where the electromagnetic part of the problem does not need to be reformulated as a circuit.

II. FORMULATION

Consider a conducting object to be modeled with distributed electromagnetic simulation, with surface S , connected to arbitrary circuits, through terminals to be defined later, excited through voltage and current sources within the circuit, and optionally illuminated by one or more electromagnetic wave excitations. Assuming a surface impedance approximation for modeling finite connectivity, the boundary condition for the electric field on the surface of the object is

$$[\mathbf{E}^s(\mathbf{J}) + \mathbf{E}^{\text{inc}}]_{\text{tan}} = \left[Z_s * \frac{\partial \mathbf{J}}{\partial t} \right]_{\text{tan}} \quad (1)$$

where \mathbf{E}^s is the scattered electric field produced by the induced equivalent surface current \mathbf{J} , \mathbf{E}^{inc} is the incident electric field, tan denotes the tangential components on S , $*$ denotes temporal convolution, and $Z_s(t)$ is the time-domain representation of surface impedance

$$Z_s(t) = \begin{cases} \sqrt{\frac{\mu}{\pi\sigma t}}, & t > 0 \\ 0, & t < 0. \end{cases} \quad (2)$$

The scattered electric field \mathbf{E}^s is written in terms of potentials

$$\mathbf{E}^s(\mathbf{J}) = -\frac{\partial \mathbf{A}}{\partial t} - \nabla \Phi \quad (3)$$

where the vector potential \mathbf{A} is defined as

$$\mathbf{A}(\mathbf{r}, t) = \frac{\mu}{4\pi} \int_S \frac{\mathbf{J}(\mathbf{r}', t - \frac{|\mathbf{r}-\mathbf{r}'|}{c})}{|\mathbf{r}-\mathbf{r}'|} ds' \quad (4a)$$

and the scalar potential Φ is given by

$$\Phi(\mathbf{r}, t) = \frac{1}{4\pi\epsilon} \int_S \frac{\rho(\mathbf{r}', t - \frac{|\mathbf{r}-\mathbf{r}'|}{c})}{|\mathbf{r}-\mathbf{r}'|} ds' \quad (4b)$$

where t denotes the observation time, \mathbf{r} and \mathbf{r}' are observation and source locations, \mathbf{J} and ρ represent the equivalent surface current density and surface charge density, respectively, and μ , ϵ , c are the permeability of, the permittivity of, and the velocity of light in, the homogeneous medium enclosing the object.

The connectivity to the circuit is introduced in the following manner. The surface S comprises of two surfaces, S_{EM} and S_{CK} such that

$$S_{EM} \cup S_{CK} = S \quad (5a)$$

and

$$S_{EM} \cap S_{CK} = \phi \quad (5b)$$

i.e., the two surfaces together yield the original surface, and the two surfaces do not have any common regions. Specifically, S_{CK} represents one electrically small portion of the total surface S and is the location where the EM object is connected to the circuit. S_{EM} is the rest portion of the total surface S . On S_{EM} the standard continuity equation relating the surface current and charge holds

$$\nabla_s \cdot \mathbf{J}(\mathbf{r}, t) + \frac{\partial \rho(\mathbf{r}, t)}{\partial t} = 0 \quad \forall \mathbf{r} \in S_{EM} \quad (6a)$$

$$\rho(\mathbf{r}, t) = - \int_0^t \nabla_s \cdot \mathbf{J}(\mathbf{r}, \tau) d\tau \quad \forall \mathbf{r} \in S_{EM} \quad (6b)$$

where ∇_s represents surface divergence. On S_{CK} , the following condition is proposed. The circuit current flowing onto S_{CK} introduces an additional source term that alters the surface current and surface charge on S . In an equivalent surface formulation, this can be the only effect of the circuit current since there is no corresponding volume current in the electromagnetic model. Moreover, this permits connection of two disparate domains, the topology-based (connectivity only) circuit domain, and the geometry-based electromagnetic domain. While wire-basis functions can also be considered as connections between the two domains [2], [3], [5], [6], the separation between the two domains is not as clear cut, and artificial parameters such as wire basis lengths, directions, and radii are needed. In the presented formulation, the altered continuity equation and a resulting voltage boundary condition for electrically small terminals are the only required links between the circuit and electromagnetic sections. Also, since the connectivity method is not based on continuity of volumetric current, the approach enables efficient surface-based electromagnetic integral equation formulations to be coupled to arbitrary circuits.

Furthermore, let S_{CK} itself be comprised of M disjoint surfaces S_{CK}^m $m = 1, \dots, M$. Each such unique subsurface S_{CK}^m is termed one of M terminals. On S_{CK}^m the modified continuity equation has the following form

$$\nabla_s \cdot \mathbf{J}(\mathbf{r}, t) + \frac{\partial \rho(\mathbf{r}, t)}{\partial t} = J_c^m(\mathbf{r}, t) \quad \forall \mathbf{r} \in S_{CK}^m \quad (7a)$$

$$\rho(\mathbf{r}, t) = - \int_0^t \nabla_s \cdot \mathbf{J}(\mathbf{r}, \tau) d\tau + \int_0^t J_c^m(\mathbf{r}, \tau) d\tau \quad \forall \mathbf{r} \in S_{CK}^m \quad (7b)$$

for $m = 1, \dots, M$, where J_c^m represents the scalar volumetric current density produced on S_{CK}^m via a circuit interconnection. As is shown next, the effect of J_c^m on the electric field is modeled through an additional equivalent surface charge. In this manner, the topology-only nature of circuits is preserved; the

direction of the interconnection current is not required. The conditions in [(6), (7)] can be combined with [(3), (4)] to generate an expression for the scattered field as follows:

$$\begin{aligned} \mathbf{E}^s(\mathbf{r}, t) = & - \frac{\partial}{\partial t} \frac{\mu}{4\pi} \int_S \frac{\mathbf{J}\left(\mathbf{r}', t - \frac{|\mathbf{r}-\mathbf{r}'|}{c}\right)}{|\mathbf{r}-\mathbf{r}'|} ds' \\ & + \nabla \frac{1}{4\pi\epsilon} \int_S \int_0^{t-|\mathbf{r}-\mathbf{r}'|/c} \frac{\nabla_s \cdot \mathbf{J}(\mathbf{r}', \tau)}{|\mathbf{r}-\mathbf{r}'|} d\tau ds' \\ & - \nabla \frac{1}{4\pi\epsilon} \sum_{m=1}^M \int_{S_{CK}^m} \int_0^{t-|\mathbf{r}-\mathbf{r}'|/c} \frac{J_c^m(\mathbf{r}', \tau)}{|\mathbf{r}-\mathbf{r}'|} d\tau ds'. \end{aligned} \quad (8)$$

The last two terms represent the contribution to the field produced by the gradient of the scalar potential, which in turn is produced by the surface equivalent charge density. The charge density itself is produced by the time integral of $\nabla_s \cdot \mathbf{J}$ over S_{EM} , and by the time integral of $\nabla_s \cdot \mathbf{J} - J_c^m$ over S_{CK}^m . Therefore, the current density introduced by the circuit interconnection produces an additional source or sink of charge that alters the time-dependent scalar potential and the resulting electric field.

If the volumetric current density J_c^m is known or can be approximated to an acceptable degree, [(1)–(8)] form a complete set of equations that can be used to solve for \mathbf{J} . However, for a coupled circuit-electromagnetic system, J_c^m is itself the result of both the circuit and the electromagnetic interactions. In this case, another self-consistent system of equations is required. This system, which will be expanded in detail later in this paper, is based on the assumption that the scalar potential produced on electrically small terminals S_{CK}^m will be equal to the circuit potential of the circuit node associated with the interconnection at S_{CK}^m . In addition, Kirchoff's Current Law will be employed for the circuit nodes connected to the terminals. To know more about J_c^m , the reader is encouraged to refer to [27]

In the following section, the expressions in [(1), (8)] and the self-consistency constraints above will be used as the basis to develop a coupled circuit-electromagnetic system of time-stepping equations. The [(1), (8)] are discretized using edge-based Rao–Wilton–Glisson (RWG) [17], [18] spatial basis functions that rely on a triangular discretization of the surface S . The RWG functions $\mathbf{f}_m(\mathbf{r})$ used to specify the spatial distribution of current density have the well-known form

$$\mathbf{f}_m(\mathbf{r}) = \begin{cases} \frac{l_m}{2A_{m+}} \boldsymbol{\rho}_{m+}, & \mathbf{r} \in T_{m+} \\ -\frac{l_m}{2A_{m-}} \boldsymbol{\rho}_{m-}, & \mathbf{r} \in T_{m-} \end{cases} \quad (9a)$$

where l_m is the length of the m th edge, $A_{m+/-}$ is the area of triangle $T_{m+/-}$, and $\boldsymbol{\rho}_{m+/-}$ is the vector from the node in triangle $T_{m+/-}$ opposite edge m to the location \mathbf{r} in triangle $T_{m+/-}$. As a consequence of the above form, the charge density in each pair of triangles is modeled as piecewise-constants as follows:

$$\nabla \cdot \mathbf{f}_m(\mathbf{r}) = \begin{cases} \frac{l_m}{A_{m+}}, & \mathbf{r} \in T_{m+} \\ -\frac{l_m}{A_{m-}}, & \mathbf{r} \in T_{m-}. \end{cases} \quad (9b)$$

For consistency with the RWG functions, the conduction current density, appearing in the last summation in (8) as an equivalent charge, will also be modeled spatially with piecewise constant

functions over each terminal triangle. The scattered field is written as

$$\begin{aligned} \mathbf{E}^s(\mathbf{r}, t) &= -\frac{\partial}{\partial t} \frac{\mu}{4\pi} \sum_{i=1}^{N_e} \int_{T_{i+} \cup T_{i-}} \frac{\mathbf{J}\left(\mathbf{r}', t - \frac{|\mathbf{r}-\mathbf{r}'|}{c}\right)}{|\mathbf{r}-\mathbf{r}'|} ds' \\ &+ \nabla \frac{1}{4\pi\epsilon} \sum_{j=1}^{N_e} \int_{T_{j+} \cup T_{j-}} \int_0^{t-|\mathbf{r}-\mathbf{r}'|/c} \frac{\nabla_s \cdot \mathbf{J}(\mathbf{r}', \tau)}{|\mathbf{r}-\mathbf{r}'|} d\tau ds' \\ &- \nabla \frac{1}{4\pi\epsilon} \sum_{m=1}^M \sum_{k=1}^{N_{p,CK}^m} \int_{T_{k,CK}^m} \int_0^{t-|\mathbf{r}-\mathbf{r}'|/c} \frac{J_{c,k}^m(\mathbf{r}', \tau)}{|\mathbf{r}-\mathbf{r}'|} d\tau ds' \end{aligned} \quad (10)$$

where N_e is the total number of triangular patches, $N_{p,CK}$ is the total number of triangular patches on all terminals, $T_{i,CK}^m$ denotes the i th triangular patch on terminal m , and T_{i+} and T_{i-} are the two patches associated with the i th edge.

Once the spatial model is chosen as above, a temporal approximation is also needed for the current density. There are a host of choices available for this. In general, the current density is expanded as

$$\mathbf{J}(\mathbf{r}, t) \cong \sum_{i=1}^{N_e} I_i(t) \mathbf{f}_i(\mathbf{r}) \quad (11a)$$

where $I_i(t)$ represents the temporal evolution of the coefficient of the i th RWG function. For clarity of explanation of the EM-circuit coupling ideas in this paper, piecewise constant temporal basis functions are chosen. However, the coupling technique and implementation are not limited to these functions. Assuming causality, the current density can be approximated as

$$\mathbf{J}(\mathbf{r}, t) \cong \sum_{i=1}^{N_e} \sum_{l=1}^{\lceil t/\Delta t \rceil} \alpha_{il} g_l \{t - t_l\} \mathbf{f}_i(\mathbf{r}) \quad (11b)$$

where the coefficients α_{il} are unknown and

$$g_l \{t - t_l\} = \begin{cases} 1, & t_l \leq t < t_{l-1} \\ 0, & \text{otherwise} \end{cases} \quad (11c)$$

with

$$t_l = (l-1)\Delta t \quad (11d)$$

where Δt is the time step discretization. The volume current density at the terminals is modeled in a manner similar to (11), albeit with piecewise constant spatial functions

$$J_c(\mathbf{r}, t) \cong \sum_{n=1}^M \sum_{k=1}^{N_{p,CK}^n} K_{nk}(t) h_{nk}(\mathbf{r}) \quad (12)$$

where $h_{nk}(\mathbf{r})$ is unity on the k th triangle of terminal n and zero otherwise. Also, $K_{nk}(t)$ represents the time dependent coefficient of $h_{nk}(\mathbf{r})$. From (1), (3), and (4), the following is obtained:

$$\left[\frac{\partial \mathbf{A}}{\partial t} + \nabla \Phi \right]_{\text{tan}} = \left[-Z_s * \frac{\partial \mathbf{J}}{\partial t} \right]_{\text{tan}} + [\mathbf{E}^i]_{\text{tan}}. \quad (13)$$

For clarity of explanation, a first-order backward Euler approximation is used for the time derivative, to obtain, at time step t_l

$$\begin{aligned} &[\mathbf{A}(\mathbf{r}, t_l) - \mathbf{A}(\mathbf{r}, t_{l-1}) + \Delta t \nabla \Phi(\mathbf{r}, t_l)]_{\text{tan}} \\ &= \left[-\Delta t Z_s * \frac{\partial \mathbf{J}(\mathbf{r})}{\partial t} (t_l) \right]_{\text{tan}} + \Delta t [\mathbf{E}^i(\mathbf{r}, t_l)]_{\text{tan}} \end{aligned} \quad (14)$$

where the temporal functional dependence in the convolution has been notationally suppressed, and the time point in parentheses represents the time point of evaluation of the temporal convolution. Using the Galerkin procedure, both sides of the above equation are tested with RWG functions $\mathbf{f}_n, n = 1, \dots, N_e$. For any specific RWG function, the testing procedure yields

$$\begin{aligned} &\langle \mathbf{f}_n, \mathbf{A}(\mathbf{r}, t_l) \rangle + \langle \mathbf{f}_n, \Delta t \nabla \Phi(\mathbf{r}, t_l) \rangle \\ &= \langle \mathbf{f}_n, \Delta t \mathbf{E}^i(\mathbf{r}, t_l) \rangle + \langle \mathbf{f}_n, \mathbf{A}(\mathbf{r}, t_{l-1}) \rangle \\ &+ \left\langle \mathbf{f}_n, -\Delta t Z_s * \frac{\partial \mathbf{J}(\mathbf{r})}{\partial t} (t_l) \right\rangle \end{aligned} \quad (15)$$

where $\langle \cdot, \cdot \rangle$ denotes a spatial dot-product. The testing of the vector potential operator yields

$$\langle \mathbf{f}_m, \mathbf{A}(\mathbf{r}, t_l) \rangle = \frac{\mu}{4\pi} \sum_{i=1}^{N_e} I_i \left(t_l - \frac{R_{mi}}{c} \right) \kappa_{mi} \quad (16a)$$

$$\kappa_{mi} = \left\langle \mathbf{f}_m(\mathbf{r}), \int_{T_{i+} \cup T_{i-}} \frac{\mathbf{f}_i(\mathbf{r}')}{|\mathbf{r}-\mathbf{r}'|} ds' \right\rangle \quad (16b)$$

and the testing of the scalar potential leads to

$$\begin{aligned} \langle \mathbf{f}_m, \nabla \Phi(\mathbf{r}, t_l) \rangle &= -\langle \nabla \cdot \mathbf{f}_m, \Phi(\mathbf{r}, t_l) \rangle \\ &= \frac{-1}{4\pi\epsilon} \left\{ \sum_{i=1}^{N_e} \lambda_{mi} \int_0^{t_l - R_{mi}/c} I_i(\tau) d\tau \right. \\ &\quad \left. - \sum_{n=1}^M \sum_{k=1}^{N_{p,CK}^n} \nu_{m,nk} \int_0^{t_l - R_{m,nk}/c} K_{nk}(\tau) d\tau \right\} \end{aligned} \quad (17a)$$

$$\lambda_{mi} = \left\langle \nabla \cdot \mathbf{f}_m(\mathbf{r}), \int_{T_{i+} \cup T_{i-}} \frac{\nabla' \cdot \mathbf{f}_i(\mathbf{r}')}{|\mathbf{r}-\mathbf{r}'|} ds' \right\rangle \quad (17b)$$

$$\begin{aligned} \nu_{m,nk} &= \left\langle \nabla \cdot \mathbf{f}_m(\mathbf{r}), \int_{T_{k,CK}^n} \frac{h_{nk}(\mathbf{r}')}{|\mathbf{r}-\mathbf{r}'|} ds' \right\rangle \\ &= \left\langle \nabla \cdot \mathbf{f}_m(\mathbf{r}), \int_{T_{k,CK}^n} \frac{1}{|\mathbf{r}-\mathbf{r}'|} ds' \right\rangle \end{aligned} \quad (17c)$$

where R_{mi} is the distance between the center of edge m and edge i , and $R_{m,nk}$ is the distance between the center of edge m and the centroid of the k th triangle on the n th terminal. Note that edge-to-edge distances are used in the formulation in order to elucidate the overall coupling scheme; in actual practice, triangle-to-triangle and quadrature point-to-quadrature point distances are used in order to estimate time delays.

The repeated computation at every time step of the temporal convolution required in (15) due to the surface impedance term is very expensive. To circumvent this, a fast recursive

method [16] for efficient computation of the convolution is implemented. The convolution is written as

$$\begin{aligned} Z_s(t_l) * \left(\frac{\partial \mathbf{J}(\mathbf{r}, t_l)}{\partial t} \right) &= \int_0^{t_l} \sqrt{\frac{\mu}{\pi\sigma\tau}} \frac{\partial \mathbf{J}(\mathbf{r}, t_l - \tau)}{\partial(t_l - \tau)} d\tau \\ &= \sqrt{\frac{\mu}{\pi\sigma}} \int_0^{t_l} \frac{1}{\sqrt{\tau}} \frac{\partial \mathbf{J}(\mathbf{r}, t_l - \tau)}{\partial(t_l - \tau)} d\tau \end{aligned} \quad (18a)$$

and is approximated with a backward Euler difference form to obtain

$$\begin{aligned} &\sqrt{\frac{\mu}{\pi\sigma}} \int_0^{t_l} \frac{1}{\sqrt{\tau}} \frac{\partial \mathbf{J}(\mathbf{r}, t_l - \tau)}{\partial(t_l - \tau)} d\tau \\ &= \chi \sum_{n=0}^{l-1} Z_0(n) [\mathbf{J}(\mathbf{r}, (l-n)\Delta t) - \mathbf{J}(\mathbf{r}, (l-n-1)\Delta t)] \end{aligned} \quad (18b)$$

where $\chi = \sqrt{\mu/\pi\sigma}$, and $Z_0(n) = \int_n^{(n+1)} d\alpha/\sqrt{\alpha}$. Exponential fitting with Prony's Method is used to approximate $Z_0(n)$ as

$$Z_0(n) = \int_n^{n+1} \frac{1}{\sqrt{\alpha}} d\alpha \approx \sum_{i=1}^N a_i e^{n\beta_i} \quad (18c)$$

where N is the number of exponentials. It was shown in [16] that good accuracy could be achieved for $N \geq 10$. Substituting (18c) into (18b) gives

$$\begin{aligned} &\chi \sum_{n=0}^{l-1} Z_0(n) [\mathbf{J}(\mathbf{r}, (l-n)\Delta t) - \mathbf{J}(\mathbf{r}, (l-n-1)\Delta t)] \\ &= \chi \sqrt{\frac{1}{\Delta t}} \sum_{i=1}^N \sum_{n=0}^{l-1} a_i e^{n\beta_i} [\mathbf{J}(\mathbf{r}, (l-n)\Delta t) - \mathbf{J}(\mathbf{r}, (l-n-1)\Delta t)] \end{aligned} \quad (18d)$$

and the testing operation transforms to

$$\begin{aligned} &\left\langle \mathbf{f}_m, -\Delta t Z_s(t_l) * \frac{\partial \mathbf{J}(\mathbf{r}, t_l)}{\partial t} \right\rangle \\ &= -\chi \sqrt{\Delta t} \sum_{i=1}^N \sum_{p=1}^P \gamma_{mk_p i} \Psi_{mk_p i}^l \end{aligned} \quad (19a)$$

$$\Psi_{mk_p i}^l = \sum_{n=0}^{l-1} a_i e^{n\beta_i} [I_{mk_p}((l-n)\Delta t) - I_{mk_p}((l-n-1)\Delta t)] \quad (19b)$$

where $\gamma_{mk_p} = \langle \mathbf{f}_m, \mathbf{f}_{k_p} \rangle$ and P is the number of edges sharing the same triangle with edge m . Also, $\Psi_{mk_p i}^l$ and $\Psi_{mk_p i}^{l-1}$ are recursively related as

$$\Psi_{mk_p i}^l = a_i [I_{mk_p}(l\Delta t) - I_{mk_p}((l-1)\Delta t)] + e^{\beta_i} \Psi_{mk_p i}^{l-1} \quad (19c)$$

Therefore, instead of computing the convolution directly, only $\Psi_{mk_p i}^l$ needs to be updated at each time step, and only one past

value is retained for the recursion. Finally, the Galerkin testing in (15) leads to the following matrix equation:

$$\begin{aligned} &\sum_{i=1}^{N_e} Z_{mi}^a(t_l) + \Delta t \sum_{i=1}^{N_e} Z_{mi}^b(t_l) + \Delta t \sum_{n=1}^M \sum_{k=1}^{N_{p,CK}^n} Q_{mnk}^a(t_l) \\ &= \Delta t F_m(t_l) + \sum_{i=1}^{N_e} Z_{mi}^a(t_{l-1}) + Z_m^c(t_l) \end{aligned} \quad (20a)$$

$$Z_{mi}^a(t_l) = \frac{\mu}{4\pi} \kappa_{mi} I_i \left(t_l - \frac{R_{mi}}{c} \right) \quad (20b)$$

$$Z_{mi}^b(t_l) = \frac{-1}{4\pi\epsilon} \lambda_{mi} \int_0^{t_l - R_{mi}/c} I_i(\tau) d\tau \quad (20c)$$

$$Q_{mnk}^a(t_l) = \frac{1}{4\pi\epsilon} \nu_{mnk} \int_0^{t_l - R_{mnk}/c} K_{nk}(\tau) d\tau \quad (20d)$$

$$F_m(t_l) = \langle \mathbf{f}_m, \mathbf{E}^{\text{inc}}(\mathbf{r}, t_l) \rangle \quad (20e)$$

$$Z_m^c(t_l) = -\chi \sqrt{\Delta t} \sum_{i=1}^N \sum_{p=1}^P \gamma_{mk_p i} \Psi_{mk_p i}^l \quad (20f)$$

for $m = 1, \dots, N_e$. In addition, the voltage matching at the terminals leads to the equation

$$\begin{aligned} &\sum_{i=1}^{N_e} Z_{nk,i}^d(t_l) + \sum_{n'=1}^M \sum_{k'=1}^{N_{p,CK}^{n'}} Q_{nk,n'k'}^b(t_l) \\ &= V_m(t_l) \end{aligned} \quad (21a)$$

$$\begin{aligned} Z_{nk,i}^d(t_l) &= \frac{-1}{4\pi\epsilon} \int_0^{t_l - R_{nk,i}/c} I_i(\tau) d\tau \\ &\times \left\langle h_{nk}(\mathbf{r}), \int_{T_{i+} \cup T_{i-}} \frac{\nabla \cdot \mathbf{f}_i(\mathbf{r}')}{|\mathbf{r} - \mathbf{r}'|} ds' \right\rangle \end{aligned} \quad (21b)$$

$$\begin{aligned} Q_{nk,n'k'}^b &= \frac{1}{4\pi\epsilon} \int_0^{t_l - R_{nk,n'k'}/c} K_{n'k'}(\tau) d\tau \\ &\times \left\langle h_{n'k'}(\mathbf{r}), \int_{T_{k',CK}^{n'}} \frac{h_{n'k'}(\mathbf{r}')}{|\mathbf{r} - \mathbf{r}'|} ds' \right\rangle \end{aligned} \quad (21c)$$

for $n = 1, \dots, M$; $k = 1, \dots, N_{p,CK}^n$ where V_m is the circuit potential at the circuit node connected to terminal m , $R_{nk,i}$ is the distance between the center of edge i and the centroid of the k th triangle on terminal n , and $R_{nk,n'k'}$ is the distance between the centroids of the k th triangle on terminal n and the k' th triangle on terminal n' . The final set of self-consistency equations relates to the application of Kirchoff's Current Law at the M nodes connected to the terminals

$$\sum_{j=1}^{\text{adj}(n)} i_j^n(t_l) = \int_{S_{CK}^n} J_c^n(t_l) ds \quad (22)$$

for $n = 1, \dots, M$ where $\text{adj}(n)$ denotes the number of nodes adjacent (neighboring) to the circuit node associated with terminal n , i_j^n is the circuit current entering node n from its j th immediate neighbor, and J_c^n is the volume conduction current density at terminal n .

The systems of [(20)–(22)] can be combined to yield the time-domain circuit electromagnetic-coupled system. The linear and nonlinear circuits connected to the terminals are modeled by modified nodal analysis (MNA). The details for the

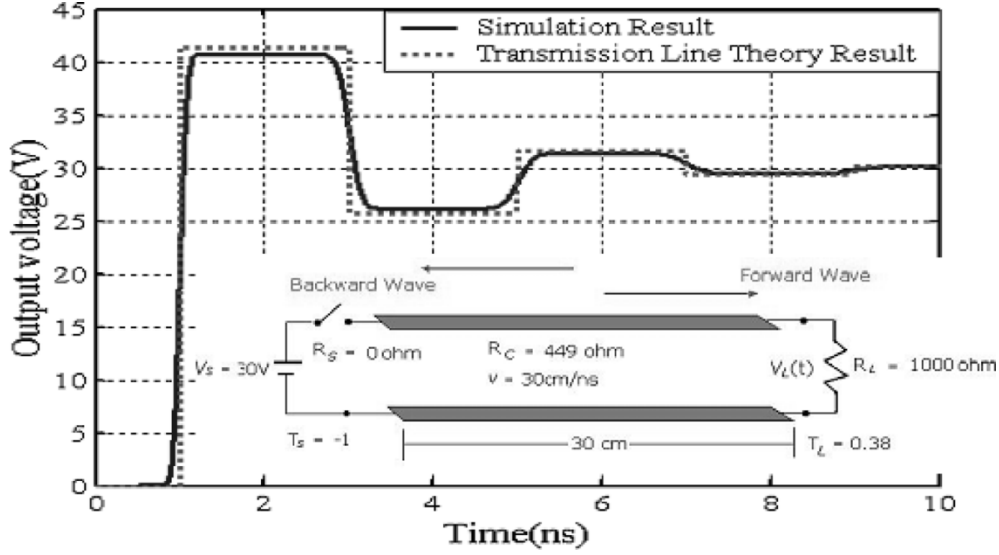


Fig. 1. Time-domain load voltage due to a step voltage applied to a transmission line, computed by transmission line theory and with the coupled time-domain simulation. The transmission line structure is shown in the inset.

linear and nonlinear stamps in the MNA matrices and related solution methods are not discussed here. The combined system has the form

$$\begin{aligned}
 & \begin{bmatrix} \overline{\mathbf{Z}}_0^{ab} & \overline{\mathbf{Q}}_0^a & \overline{\mathbf{0}} \\ \overline{\mathbf{Z}}_0^c & \overline{\mathbf{Q}}_0^b & \overline{\mathbf{C}} \\ \overline{\mathbf{0}} & \overline{\mathbf{C}}^T & \overline{\mathbf{MNA}}_0 \end{bmatrix} \begin{bmatrix} \mathbf{I}(t_j) \\ \mathbf{J}_c(t_j) \\ \mathbf{ckt}(t_j) \end{bmatrix} \\
 &= \sum_{i=1}^j \begin{bmatrix} \overline{\mathbf{Z}}_i^{ab} & \overline{\mathbf{Q}}_i^a & \overline{\mathbf{0}} \\ \overline{\mathbf{Z}}_i^c & \overline{\mathbf{Q}}_i^b & \overline{\mathbf{0}} \\ \overline{\mathbf{0}} & \overline{\mathbf{0}} & \overline{\mathbf{MNA}}_i \end{bmatrix} \begin{bmatrix} \mathbf{I}(t_{j-i}) \\ \mathbf{J}_c(t_{j-i}) \\ \mathbf{ckt}(t_{j-i}) \end{bmatrix} \\
 &+ \begin{bmatrix} \mathbf{src}_{EM}(t_j) \\ \mathbf{0} \\ \mathbf{src}_{CK}(t_j) \end{bmatrix} \quad (23a)
 \end{aligned}$$

$$\begin{aligned}
 \mathbf{I}(t_j) &= \begin{pmatrix} I_1(t_j) \\ I_2(t_j) \\ \vdots \\ I_{N_e}(t_j) \end{pmatrix} \\
 \mathbf{J}_c(t_j) &= \begin{pmatrix} \mathbf{K}_1(t_j) \\ \mathbf{K}_2(t_j) \\ \vdots \\ \mathbf{K}_M(t_j) \end{pmatrix} \\
 \mathbf{K}_n(t_j) &= \begin{pmatrix} K_{n1}(t_j) \\ K_{n2}(t_j) \\ \vdots \\ K_{nN_{p,CK}^n}(t_j) \end{pmatrix}, \quad n = 1, \dots, M \quad (23b)
 \end{aligned}$$

where the submatrix superscripts refer to the type of matrices generated earlier. The vector $\mathbf{src}_{EM}(t_j)$ represents the incident field tested with each RWG function, and the vector $\mathbf{src}_{CK}(t_j)$ denotes the values of circuit sources. Typically, the history of MNA blocks appearing in each matrix on the right-hand side is limited to very few (one in the case of time-independent linear *RLC* circuits) past time steps. The matrix $\overline{\mathbf{C}}$ is a sparse bipolar adjacency matrix that is used for enforcing Kirchoff's Voltage and Current Laws at the circuit nodes connected to the terminals.

Depending on the choice of time step, (23) can be implemented as an implicit or explicit solution process [18], [19]. The implicit method, developed to remove late time instabilities [8], [9], [24]–[26] associated with TDIE, uses a time step greater than the smallest distance between two triangle centroids divided by the speed of light. The interaction from any source triangle whose centroid is located within the sphere centered at the centroid of the observer triangle, of radius of the time step multiplied by the speed of light is assumed to be instantaneous. This method ensures that the left-hand side matrix to be inverted is still sparse, but improves stability compared to an explicit scheme where only self-interactions are considered instantaneous. However one drawback of the implicit method is its dissipation effect [8], [9] when time step is large. To satisfy both high-resolution simulation requirements and late time stability, two constraints are kept in mind when choosing the time step. First, the time step should be small enough to accurately describe the highest frequency component in the time domain signal. Second, the time step should be large enough to ensure the implicitness of the system for enabling late time stability. Due to its high sparsity nature of the left-hand coupled matrix, it can be inverted efficiently with a Sparse LU decomposition. For nonlinear circuits, a Newton–Raphson loop is implemented at each time step to consistently solve circuit and electromagnetic unknowns.

III. NUMERICAL RESULTS

A validation test is performed on the coupled time domain solver by a simulation of load voltage variation on a transmission line structure (inset of Fig. 1). The two conducting lines are 1-mm wide, 30-cm long, and separated by 10 mm. The characteristic impedance of this structure is calculated to be 449 Ω [20]. The two lines are assumed to be perfectly conducting. A step voltage source with an amplitude of 30 V is used to excite the structure, and the voltage source and load impedance are modeled with a small MNA inclusion in the coupled system as

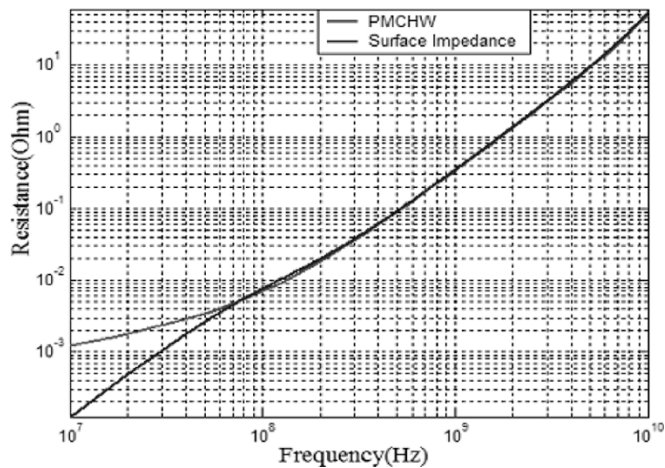


Fig. 2. Resistance variation of a lossy copper cylinder with frequency.

in (22). The resulting load voltage $V_L(t)$ is computed using the transmission line equations and with the coupled time-domain solver. Fig. 1 demonstrates the close match between the two results, with the unrealistically sharp voltage transitions of the idealized transmission line model replaced by smoother changes due to dispersion effects as predicted by the time-domain solver. The slight difference in magnitude between the two results is due to the dissipation effect of the implicit method.

The surface impedance model implemented in this paper is a good approximation to model lossy conductors with high conductivity at high frequencies. As is well known from frequency domain versions, this model will not correctly predict resistance value at very low frequencies where the skin depth is larger than the cross section of the conductors. To verify the surface impedance model implemented in our solver for the frequencies and conductivities of interest, we compare our simulation result (by performing a Fourier transform) with that from a rigorous frequency domain two-region Poggio, Miller, Chang, Harrington, Wu, and Tsai (PMCHWT) formulation, which is capable of accurate lossy material modeling down to dc [23].

The first simple comparison is the frequency variation of resistance of a lossy copper conductors (conductivity 5.8×10^7 S/m) cylinder. The diameter of the cylinder is 1 mm and its length is 5 mm. Fig. 2 indicates the two methods have very good match at 70 MHz and higher frequencies. For frequencies from 70 MHz down to dc, as expected, the simulation result from the surface impedance model deviates from that generated by the exact PMCHWT formulation. The second comparison is the variation of inductance of a lossy copper inductor (conductivity 5.8×10^7 S/m) with frequency. The thickness of the inductor is 1 mm. Fig. 3 shows excellent match between the two methods.

The third example considers a multiple via structure, as shown in the inset of Fig. 4. The requirement is to find the coupling crosstalk between the active signal pin and the passive signal pin, and to find the impact of ground pins on the crosstalk. The top end of the active pin is terminated by a $52\text{-}\Omega$ resistor

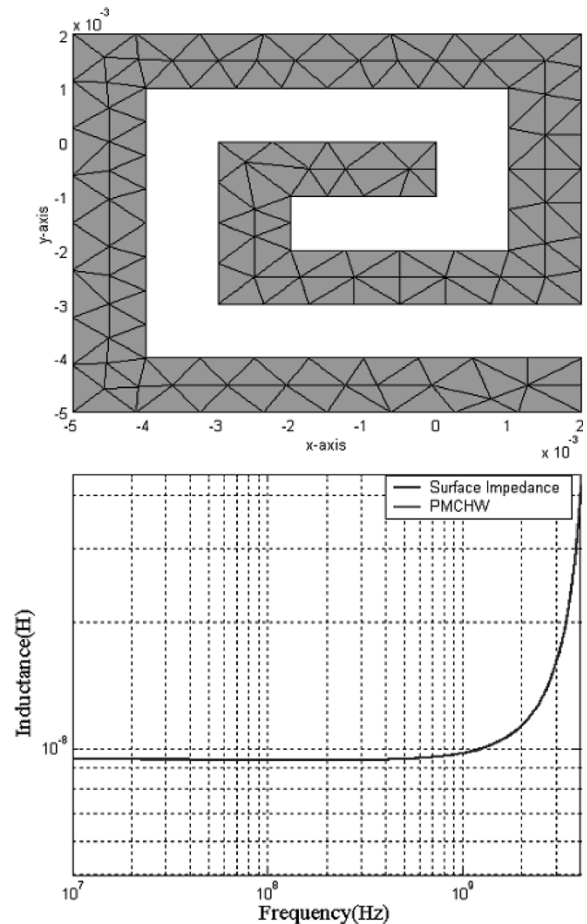


Fig. 3. (Top) Top view of the spiral inductor. (Bottom) Inductance variation of a lossy copper inductor with frequency.

and the resistor is connected to the top ground plane through a ramp voltage source. The bottom end of the active pin is also terminated by a $52\text{-}\Omega$ resistor, and the resistor is connected to the bottom ground plane. The passive pin is connected to the top and bottom ground planes in the same manner through two resistors, with no voltage source. The structure is embedded in a dielectric of relative permittivity equal to four. The simulation shows the voltage drop across the top end (near) resistor and bottom end (far) resistor of the active pin and passive pin, for two cases. In the first case, there are six ground pins around the two signal pins. In the second case, there are 20 ground pins around the two signal pins. In both cases, the multiple via structure are copper with (conductivity 5.8×10^7 S/m). From the simulation result, it is apparent that the crosstalk was dramatically decreased when more ground pins were added. The reason for decreased crosstalk is that the return current path is more localized and shorter when nearby ground pins are added between the ground planes, thus reducing inductive effects.

The ACES IEEE/EMC Society TC9 challenging problems have been designed to challenge various modeling techniques. One of the 2001 challenging problems—"Differential Pair over Split Plane" [21] (Fig. 5, top) is used to test the coupled solver

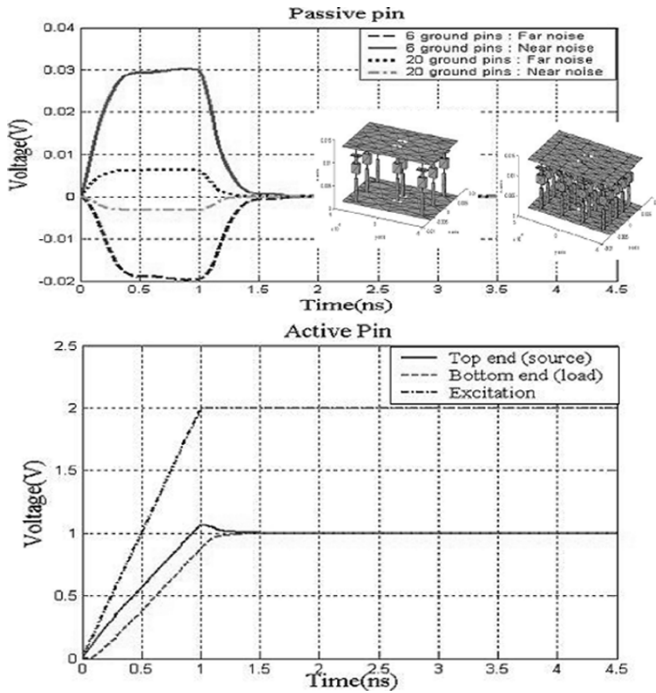


Fig. 4. (Top) Near and far end noise voltage waveforms across a victim via due to an active via in the presence of grounding pins. Inset: structures with six and 20 grounding pins. The active and victim pins are located in the center of the two-plane structure. (Bottom) Voltage excitation and voltage drop at two ends of active pin.

and also to compare the simulation with that from PEEC modeling technique [22]. In this example, a ground plane with or without split is located on the left-hand side. A driver consisting of two trapezoidal voltage sources with rising and falling time of 200 ps, roof time of 600 ps, and zero internal impedance, delivers a differential mode signal to two symmetrical lines. For the split ground plane case, a decoupling capacitor may be placed across the split. The decoupling capacitor is equivalent to a series connection of a 1-nF capacitor, a 2-nH inductor, and a 0.03- Ω resistor. The pair of wires extend for 1 m, and the ends of the differential lines are terminated by a 100- Ω resistor. The conductors are assumed to be perfectly conducting. The task is to find the voltage between Line+ and CM Ground point on plane for the following three cases:

- 1) no split in plane;
- 2) split in plane and no decoupling capacitor;
- 3) split in plane and with decoupling capacitor.

Fig. 5 (bottom) shows the simulation results obtained with the coupled solver, and the results match well with those in [22].

The final example demonstrates the ability of the coupled integral equation solver to address distributed EM simulation, nonlinear circuit models and circuit excitations, and EMI/EMC excitation in a transparent and integrated manner). Fig. 6, top, shows the structure, which includes bent co-planar copper conductors (conductivity 5.8×10^7 S/m) connected to a voltage source and to a nonlinear transistor inverter circuit, with appropriate terminations on the other lines as shown. Also present is an incoming pulse that models the disruptive effect of a large EMI/EMC excitation. A trapezoidal voltage source of peak 10 V

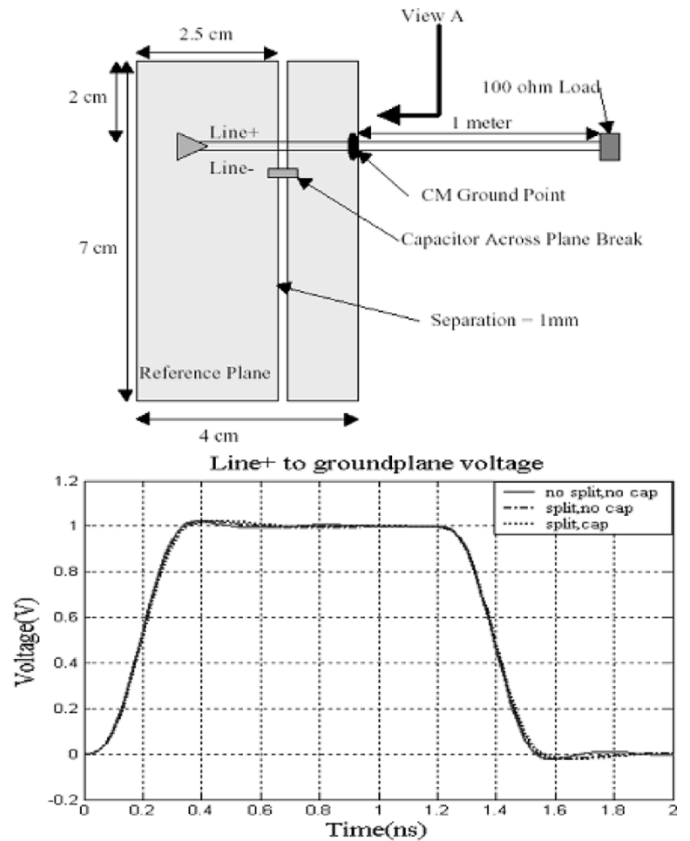


Fig. 5. (Top) Split ground plane with a loaded differential pair, with a connecting nonideal capacitor. (Bottom) Positive reference line voltage at point CM with and without the capacitor, and with and without the split.

with rising and falling time of 200 ps, roof time of 400 ps, is applied to the lines connecting to the nonlinear circuit. The EMI pulse is a Gaussian pulse with an electric field of the form $\mathbf{E}(\mathbf{r}, t) = (A\hat{\mathbf{E}}_0/\sqrt{\pi}) \exp\{-(4/T)^2(t-T_0 - \mathbf{r} \cdot \hat{\mathbf{k}}/c)^2\}$, $A = 10$ k(V/m), $\hat{\mathbf{E}}_0 = -1/2\hat{\mathbf{x}} - 1/2\hat{\mathbf{y}} - \sqrt{2}/2\hat{\mathbf{z}}$, $\hat{\mathbf{k}} = -\sqrt{2}/2\hat{\mathbf{x}} + \sqrt{2}/2\hat{\mathbf{y}}$, $T = 0.01$ LM, $T_0 = 0.1$ LM, where LM denotes time in light-meters. The simulation, shown in Fig. 6 (bottom) are the output voltages of the inverter without and with the disruption of the incident pulse. With the disruption of the strong incident pulse, the output of the inverter is severely distorted; with no EMI pulse, the output voltage of the inverter is a delayed and thresholded version of the voltage applied to the multiconductor bends. However, the EMI pulse changes the switching times as well as causes a false pulse in the output voltage, leading to potentially spurious and mistimed circuit switching.

IV. CONCLUSION

A coupling scheme to simultaneously time-step MNA and TDIE equations was developed in this paper in order to model complex circuits with different levels of hierarchy. The method enables nonlinear simulation as well as EMI/EMC modeling, and potentially can serve as a complement to the PEEC approach for modeling skin effects and arbitrarily shaped microelectronic package and chip structures. The method obviates the need and problems associated with time-domain circuit realizations

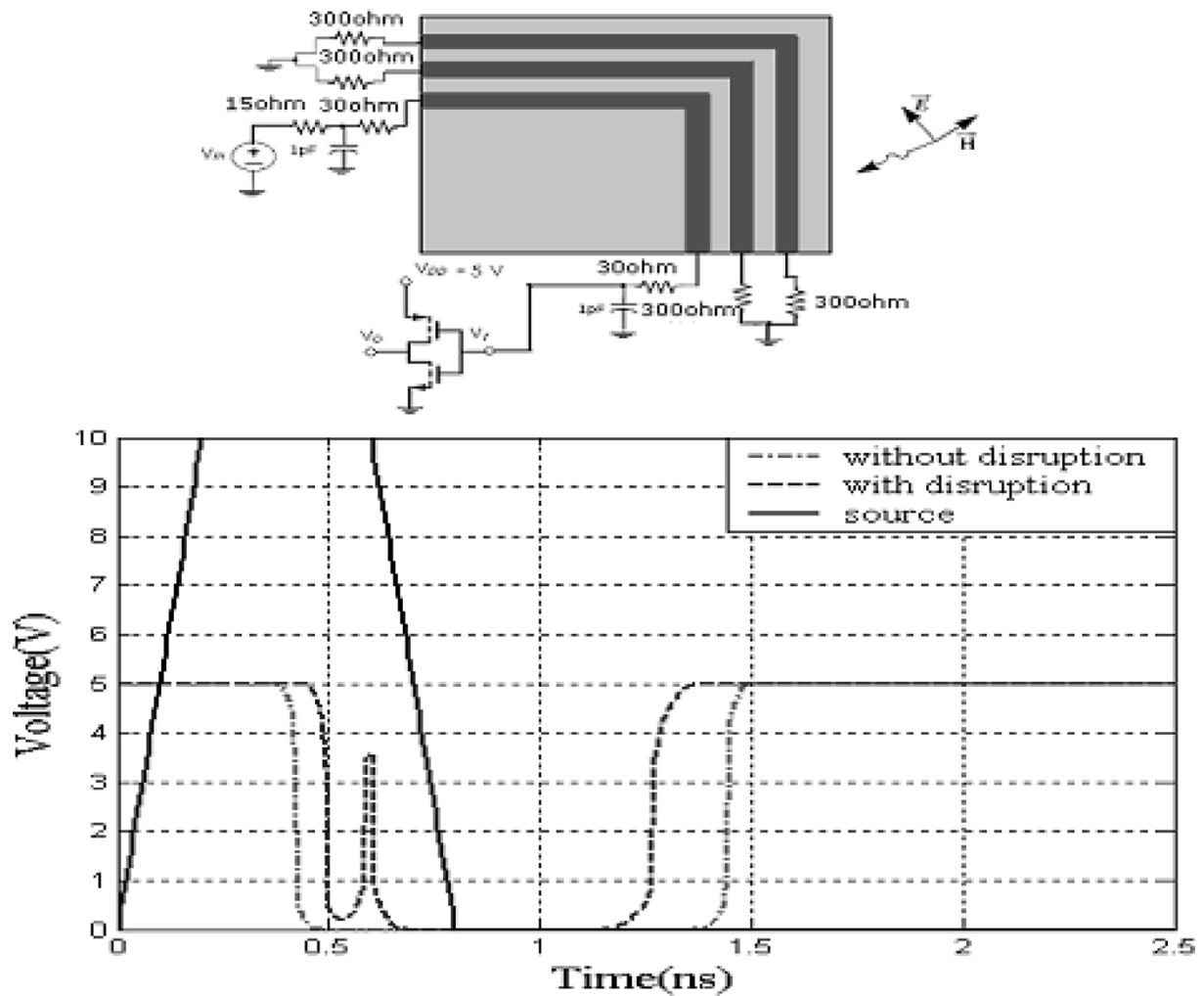


Fig. 6. (Top) Nonlinear circuit connected to bent conductors, with circuit and EMI pulse excitation. (Bottom) Output voltage at inverter with and without EMI pulse disruption. The circuit voltage input is a trapezoidal pulse.

of electromagnetic components since it presents a complete coupled simulation approach.

ACKNOWLEDGMENT

The authors would like to thank S. Chakraborty for his help with providing frequency domain PMCHW simulation results used to verify our surface impedance model.

REFERENCES

- [1] I. Erdin, M. S. Nakhla, and R. Achar, "Circuit analysis of electromagnetic radiation and field coupling effects for networks with embedded full-wave modules," *IEEE Trans. Electromagn. Compat.*, vol. 42, no. 4, pp. 449–460, Nov. 2000.
- [2] K. Aygun, B. Shanker, and E. Michielssen, "Analysis of nonlinearly loaded antennas and circuits using the multilevel plane wave time domain algorithm," in *Proc. Int. Conf. Electromagnetics Advanced Applications*, Turin, Italy, Sep. 1999, pp. 741–744.
- [3] K. Aygun, B. Fischer, A. Cangellaris, and E. Michielssen, "Fast time domain analysis of nonlinearly loaded printed circuit board structures," in *National Radio Science Meeting*, Boulder, CO, Jan. 2002.
- [4] A. A. Ergin, B. Shanker, and E. Michielssen, "The plane-wave time-domain algorithm for the fast analysis of transient wave phenomena," *IEEE Antennas Propag. Mag.*, vol. 41, no. 4, pp. 39–52, Sep. 1999.
- [5] K. Aygun, B. Shanker, A. A. Ergin, and E. Michielssen, "A two-level plane wave time-domain algorithm for fast analysis of EMC/EMI problems," *IEEE Trans. Electromagn. Compat.*, vol. 44, no. 1, pp. 152–164, Feb. 2002.
- [6] —, "A fast time domain integral equation technique for analyzing EMC/EMI problems," in *Proc. IEEE Int. Symp. Antennas and Propagation Soc.*, vol. 2, 1999, pp. 1366–1369.
- [7] A. E. Ruehli, "Equivalent circuit models for three dimensional multi-conductor systems," *IEEE Trans. Microw. Theory Tech.*, vol. MTT-22, no. 3, pp. 216–221, Mar. 1974.
- [8] W. Pinello, A. C. Cangellaris, and A. Ruehli, "Hybrid electromagnetic modeling of noise interactions in packaged electronics based on the partial-element equivalent-circuit formulation," *IEEE Trans. Microw. Theory Tech.*, vol. 45, no. 10, pp. 1889–1896, Oct. 1997.
- [9] W. Pinello, A. Ruehli, and A. Cangellaris, "Stabilization of time domain solutions of EFIE based on partial element equivalent circuit models," in *Proc. IEEE Antennas and Propagation Soc. Int. Symp. Dig.*, vol. 2, 1997, pp. 966–969.
- [10] P. J. Restle, A. E. Ruehli, S. G. Walker, and G. Papadopoulos, "Full-wave PEEC time-domain method for the modeling of on-chip interconnects," *IEEE Trans. Computer-Aided Design Integr. Circuits Syst.*, vol. 20, no. 7, pp. 877–866, Jul. 2001.
- [11] M. A. Leontovich, *Investigations on Radiowave Propagation*. Moscow, USSR: Printing House of USSR Academy Science, 1948, pt. II.
- [12] T. B. A. Senior, "Impedance boundary conditions for imperfectly conducting surface," *Appl. Sci. Res.*, vol. 8(B), pp. 418–436, 1960.

- [13] J. G. Maloney and G. S. Smith, "The use of surface impedance concepts in the finite-difference time-domain method," *IEEE Trans. Antennas Propag.*, vol. 40, no. 1, pp. 38–48, Jan. 1992.
- [14] K. S. Oh and J. E. Schutt-Aine, "An efficient implementation of surface impedance boundary conditions for the finite-difference time-domain method," *IEEE Trans. Antennas Propag.*, vol. 43, no. 1, pp. 660–666, Jan. 1995.
- [15] C. R. Paul, *Analysis of Multiconductor Transmission Lines*. New York: Wiley, 1994.
- [16] K. S. Kunz and R. J. Luebbers, *The Finite Difference Time Domain Method in Electromagnetics*. Boca Raton, FL: CRC, 1993.
- [17] S. M. Rao and D. R. Wilton, "Transient scattering by conducting surfaces of arbitrary shape," *IEEE Trans. Antennas Propag.*, vol. 39, no. 1, pp. 56–61, Jan. 1991.
- [18] S. M. Rao, *Time Domain Electromagnetics*. San Diego, CA: Academic, 1999.
- [19] S. P. Walker, "Developments in time-domain integral-equation modeling at imperial college," *IEEE, Antennas Propag. Mag.*, vol. 39, no. 1, pp. 7–19, Feb. 1997.
- [20] E. C. Robert, *Foundation for Microwave Engineering*. New York: McGraw-Hill, 1992.
- [21] B. Archambeault and A. Ruehli, "Introduction to 2001 special challenging EMC modeling problems," in *Proc. IEEE Int. Symp. Electromagnetic Compatibility*, vol. 2, 2001, pp. 799–804.
- [22] A. E. Ruehli, J. Esch, J. S. Zhao, and C. W. Chew, "Solution of large differential signal problem using two different integral equation based methods," in *Proc. IEEE Int. Symp. Electromagnetic Compatibility*, vol. 2, 2001, pp. 815–820.
- [23] S. Chakraborty and V. Jandhyala, "Accurate computation of vector potentials in lossy media," *Microw. Opt. Technol. Lett.*, vol. 36, pp. 359–363, 2003.
- [24] J. E. Garret, A. E. Ruehli, and C. R. Paul, "Accuracy and stability improvements of integral equation models using the partial element equivalent circuit (PEEC) approach," *IEEE Trans. Antennas Propag.*, vol. 46, no. 12, pp. 1824–1832, Dec. 1998.
- [25] G. Manara, A. Monorchio, and R. Reggiannini, "A space-time discretization criterion for a stable time-marching solution of the electric field integral equation," *IEEE Trans. Antennas Propag.*, vol. 45, no. 3, pp. 527–532, Mar. 1997.
- [26] M. J. Bluck and S. P. Walker, "Time-domain BIE analysis of large three-dimensional electromagnetic scattering problems," *IEEE Trans. Antennas Propag.*, vol. 45, no. 5, pp. 894–901, May 1997.
- [27] Y. Wang, D. Gope, V. Jandhyala, and C. J. R. Shi, "Generalized Kirchoff's current and voltage law formulation for coupled circuit-electromagnetic simulation with surface integral equations," *IEEE Trans. Microw. Theory Tech.*, vol. 52, no. 7, pp. 1673–1682, Jul. 2004.



Chuanyi Yang (M'02) received the B.S. degree in physics from Jilin University, Changchun, China, in 1998 and the M.S. degree in electrical engineering from University of Washington, Seattle, in 2003. He is currently working toward the Ph.D. degree in electrical engineering at University of Washington.

From 1997 to 1999, he was a Research Assistant at the National Laboratory of Super-Hard Materials, Jilin University, where he was involved with synthesis and study on nanomaterials. Since 2001, he has been a Graduate Research Assistant at the Applied Computational Electromagnetics Laboratory, University of Washington. In the Summer of 2004, he worked at the Thomas J. Watson Research Center, IBM, Yorktown Heights, NY, on high-speed electrical interconnect and package modeling. His research interests include computational EM applied to mixed-signal circuit simulation, signal integrity for high-speed digital/analog circuit, and electromagnetic interference and compatibility.



Vikram Jandhyala (S'91–M'00–SM'03) received the B.Tech. degree in electrical engineering from the Indian Institute of Technology (IIT), Delhi, India, in 1993, and the M.S. and Ph.D. degrees from the University of Illinois, Urbana-Champaign, in 1995 and 1998, respectively. As part of his graduate work, he codeveloped the steepest descent fast-multipole method for rapid simulation of a large class of EM problems.

From 1998 to 2000, he was a Research and Development Engineer with the Ansoft Corporation, Pittsburgh, PA. He was involved in the acceleration of Ansoft's integral-equation solvers, and codeveloped a fast multipole-based extraction tool in Ansoft's SPICElink versions released in 1999 and 2000. Since 2000, he has been an Assistant Professor with the Department of Electrical Engineering, University of Washington, Seattle. He directs the Applied Computational Electromagnetics Laboratory, with research interests and projects in several areas of computational electromagnetics, including fast solvers and integral-equation formulations in the frequency and time domains, high-speed circuits and devices, coupled multiphysics simulation, novel materials, and propagation. He has visiting research status with the Lawrence Livermore National Laboratories, Livermore, CA. He has authored or coauthored over 70 journal and conference papers.

Dr. Jandhyala is a Full Elected Member of the International Scientific Radio Union (URSI) Commission B. He has served as a Reviewer for several IEEE journals and conferences and national and international proposal panels. He is on the Technical Program Committee of the IEEE Design Automation Conference and the IEEE Antennas and Propagation Society (IEEE AP-S) Symposium. He was a recipient of the 2001 National Science Foundation (NSF) CAREER grant, a 1998 Outstanding Graduate Research Award presented by the University of Illinois, and a 1996–1997 IEEE Microwave Graduate Fellowship.